ADVANCED FUNCTIONAL MATERIALS
www.afm-journal.de

Phosphorous Pentasulfide as a Novel Additive for High-Performance Lithium-Sulfur Batteries

*Zhan Lin, Zengcai Liu, Wujun Fu, Nancy J. Dudney, and Chengdu Liang**

Lithium-sulfur (Li-S) batteries suffer from rapid capacity decay and low energy efficiency because of the low solubility of lithium sulfide (Li_2S) in organic solvents and the intrinsic polysulfide shuttle phenomenon. Here, a novel additive, phosphorus pentasulfide (P_2S_5) in organic electrolyte, is reported to boost the cycling performance of Li-S batteries. The function of the additive is two-fold: 1) P_2S_5 promotes the dissolution of Li_2S and alleviates the loss of capacity caused by the precipitation of Li_2S and 2) P_2S_5 passivates the surface of lithium metal and therefore eliminates the polysulfide shuttle phenomenon. A Li-S test cell demonstrates a high reversible capacity of 900–1350 mAh g^{-1} and a high coulombic efficiency of ≥90% for at least 40 stable cycles at 0.1 C.

1. Introduction

As a byproduct of the petroleum refining process, elemental sulfur (S) is inexpensive, abundant and nontoxic. With a high theoretical capacity of 1675 mAh g^{-1} of elemental sulfur, the combination of lithium metal as the anode and elemental sulfur as the cathode provides a specific energy density of 2500 Wh kg^{-1}.[1] For this reason, the combination of lithium and sulfur has been considered as one of the most promising battery chemistries for the next generation of high energy batteries.[2] Despite considerable advantages of Li-S batteries, there are key challenges associated with Li-S battery chemistry that uses liquid organic electrolytes: 1) S and its solid discharge products are neither ionic nor electronic conductors. To enable the electrochemical reaction of sulfur cathode, various carbon materials and conducting polymers have been investigated as the electronic conductors for the sulfur cathode. Polar organic solvents, particularly ether-type solvents that have a high solubility for lithium polysulfides, have been used as the electrolytes for Li-S batteries. The high solubility of lithium polysulfides in the organic solvents circumvents the low ionic conductivity of lithium polysulfides, which are intermediates of the charge and discharge processes. 2) The intrinsic polysulfide shuttle corrodes the lithium anode, carries sulfur species from the cathode to anode and therefore causes the loss of active materials, and leads to low coulombic and poor energy efficiencies.[3] The polysulfide shuttle results from a series of chemical reactions between the cathode and anode through the migration of polysulfides in the liquid electrolytes. These chemical reactions result in undesirable self-discharge.

The rapid capacity decay in Li-S batteries is closely related to the polysulfide shuttle. To alleviate the capacity decay, various porous materials and conductive polymers were investigated to reduce the polysulfide shuttle by restraining polysulfides at the cathode through physical or chemical absorption.[4] A similar approach has also been conducted on graphene oxide. The functional groups at the surface of high surface area graphene oxide chemically absorb the sulfur species and therefore reduce the concentration of polysulfides in the organic electrolytes. When combined with a highly viscous electrolyte of ionic liquid, the sulfur cathode can be cycled for 50 cycles at 0.1 C with a reversible capacity of 950–1400 mAh g^{-1}.[5] Nevertheless, any of the known chemical or physical absorption approaches cannot completely stop the leaching of polysulfides from the cathode. As long as there are any polysulfides dissolving in the electrolytes, the migration of sulfur species through polysulfide shuttle is inevitable. Since the polysulfide shuttle involves reactions at both the cathode and anode, protection of the lithium to block the chemical reaction path at the anode can be as effective in eliminating the polysulfide shuttle as confining sulfur species at the cathode. As an additive in non-aqueous electrolytes, lithium nitrate ($LiNO_3$) reacts with metallic lithium to form a rigid passivation layer that functions as a physical barrier to block the chemical reactions of polysulfides with the lithium anode.[6] The passivation of lithium anode arises from a combination of the decomposition of organic solvents and lithium salts. $LiNO_3$ was identified as the critical component to form a protective surface film in Li-S batteries.[7] The efficacy of protecting lithium anode by $LiNO_3$ was confirmed by a number of publications from different research groups. Improved coulombic efficiency and cycling performance were observed in Li-S batteries with $LiNO_3$ as an electrolyte additive.[8]

Besides the polysulfide shuttle, the sluggish electrochemical reaction of lithium sulfide and lithium disulfide is also accountable for the rapid capacity decay of Li-S batteries. High sulfur loading and limited volume of organic electrolytes result in the precipitation of less soluble lithium sulfide and lithium

Z. Lin, N. J. Dudney
Materials Science and Technology Division
Oak Ridge National Laboratory
Oak Ridge, TN 37831-6124, USA
Z. Liu, W. Fu, C. Liang
Center for Nanophase Materials Sciences
Oak Ridge National Laboratory
Oak Ridge, TN 37831-6493, USA
E-mail: liangcn@ornl.gov

DOI: 10.1002/adfm.201200696

disulfide that often cause failure of Li-S batteries.[9] Although lithium sulfide can be electrochemically charged with intimate contact to carbon in all-solid batteries, the charge/discharge must be conducted at elevated temperatures.[10] Metal additives were employed to enhance the conductivity of Li_2S-based cathode with limited success.[11] To accelerate the cycling of lithium sulfide, lithium bromide can be used as an additive in liquid electrolytes to chemically convert the insoluble lithium sulfide back to lithium polysulfide in the charging cycle.[12] However, the incompatibility of corrosive bromine produced at the cathode with the battery components prohibits the usage of lithium bromide in Li-S batteries.

In this work, we report the effect of phosphorus pentasulfide (P_2S_5) as an electrolyte additive for Li-S batteries. We found that P_2S_5 is able to form complexes with lithium sulfide and lithium polysulfide. These complexes are soluble in organic solvents and facilitate the electrochemical reactions. P_2S_5 serves two functions in the Li-S batteries: it prevents the precipitation of lithium sulfide and lithium disulfide by forming complexes and it passivates the surface of lithium metal to reduce the polysulfide shuttle. In addition, complexes of P_2S_5 with lithium sulfide and polysulfides are non-corrosive and compatible with all cell components.

2. Results and Discussion

2.1. P_2S_5 Improves the Cycling Performance of Li-S Batteries

The dissolution of sulfur species in liquid electrolyte is a salient characteristic of Li-S batteries. The solubility of lithium sulfide and lithium polysulfide in the liquid electrolyte directly affects the cycling performance of the electrochemical cell. Therefore, the weight ratio of sulfur to solvent was carefully controlled at 1:10 for each cell to ensure a fair comparison of the experimental and control cells. These cells were intentionally tested at a slow rate of 0.1 C to observe the polysulfide shuttle. Shown in **Figure 1**A is the cycling performance of the Li-S test cells with and without P_2S_5. The experimental cell that contains P_2S_5 outperformed the control cell that contains no P_2S_5. The initial discharge capacity (based on the mass of S loading) of the experimental cell was 1122 mAh g^{-1} and increased to the highest discharge capacity of 1334 mAh g^{-1} at the 4th cycle, which is about 80% of sulfur utilization based on the theoretical maximum 1675 mAh g^{-1}. Slight capacity fading was observed before the 20th cycle. The capacity was stabilized at above 900 mAh g^{-1} after 20 cycles, about 70% of the initial highest value (1334 mAh g^{-1}). The experimental cell had a high coulombic efficiency of 98% at the first 20 cycles. Such a high coulombic efficiency indicates a suppression of the polysulfide shuttle, which has been proven to be the main cause of low coulombic efficiency in Li-S cells. A slight decline in coulombic efficiency was observed after 20 cycles. The coulombic efficiency of the experimental cell stabilized at over 90% for the entire range of cycling. Of striking contrast, the capacity of the control cell without P_2S_5 dramatically decreased from the initial capacity of 1064 mAh g^{-1} to 406 mAh g^{-1} at the 6th cycle. The coulombic efficiencies of the first 6 cycles are all below 80%. The low coulombic efficiency in the control cell is caused by severe polysulfide shuttle.

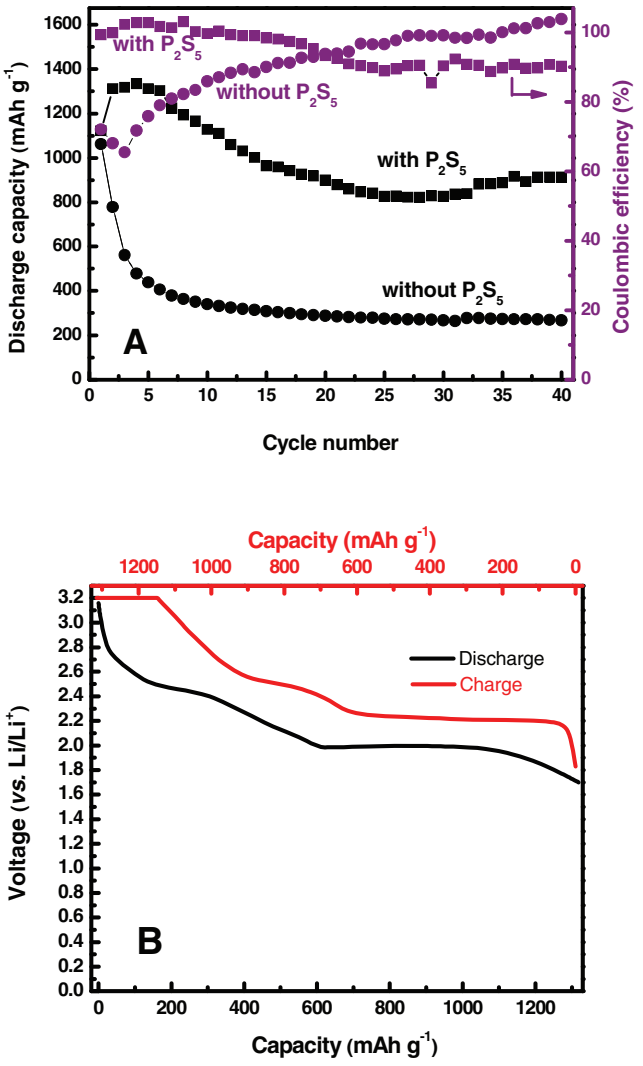

Figure 1. A) Cycling performance of Li-S batteries with/without P_2S_5 and B) representative voltage profile of Li-S with P_2S_5 additive.

Figure 1B shows the voltage profile of a representative cycle of the Li-S cell with P_2S_5. The discharge curve has two voltage plateaus at 2.4 and 2.0 V, which correspond to the reduction of long chain polysulfides (S_x^{2-}, $4 \le x$) and short chain polysulfides (S_x^{2-}, $x \le 4$). The ratio of the high plateau at 2.4 V to the low plateau at 2.0 V is exactly 1:3. The same ratio of the plateau at high potential (2.5 V) to the plateau at low potential (2.2 V) was observed at the charging cycle. The charge/discharge of a S_8 molecule involves the transfer of 16 electrons. The first 4 electrons were transferred at the high plateau and the remaining 12 electrons were transferred at the low plateau. The polysulfide shuttle carries the long-chain polysulfides from the cathode to the anode and therefore breaking the balance of the 1:3 ratio of the plateaus: at the discharge cycle, the loss of long-chain polysulfides shortens the high plateau, while at the charging cycle, the loss of long-chain polysulfides prolongs the high plateau. The constant ratio of 1:3 of these plateaus at the charge/discharge cycles and the high coulombic efficiency of the experimental cell prove that the polysulfide shuttle has been

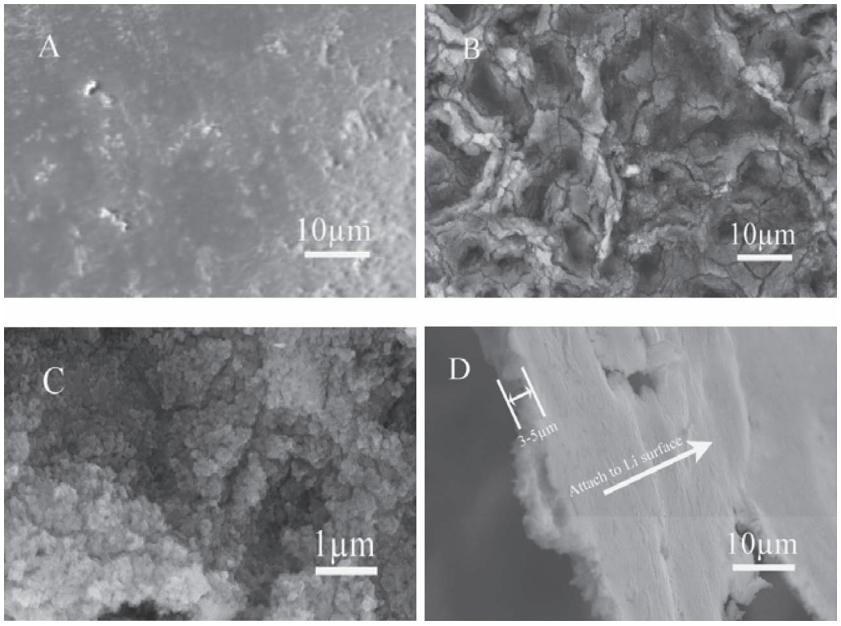

Figure 2. SEM images of A) pristine metallic Li anode, B,C) the top surface of the passivation layer on cycled lithium anode at low and high magnifications, and D) the cross-section of the passivation layer peeled off from the lithium anode cycled with P_2S_5 in the electrolyte. The arrow indicates the bottom side of the passivation layer that was in contact with the lithium metal.

completely blocked. The ideal 1:3 ratio of the plateaus was not observed in the control cell. Therefore, P_2S_5 is the critical component for blocking the polysulfide shuttle in Li-S batteries.

2.2. Super-Ionic Conductor Protects the Lithium Anode

The effect of P_2S_5 in Li-S cells is akin to $LiNO_3$, an electrolyte additive that protects metallic lithium anode in Li-S batteries. A passivation layer was observed on the lithium metal surface after the first cycle in an electrolyte that contains P_2S_5. Compared to the smooth surface of pristine metallic lithium (**Figure 2**A), the lithium anode was significantly roughened after the first cycle (Figure 2B). A close examination of the roughened surface revealed a passivation layer that consisted of granular particles less than 100 nm (Figure 2C). When peeled off of the lithium anode surface, the bottom of the passivation layer was dense and smooth (Figure 2D). The thickness estimated from the cross-section using scanning electron microscopy (SEM) was about 3 to 5 micrometers. There is no doubt that such a dense passivation layer can efficiently block access of the polysulfide to the underlining metallic lithium and eliminate the polysulfide shuttle. This passivation layer explains the high coulombic efficiency of the experimental cell.

The chemical composition of the passivation layer was checked by energy-dispersive X-ray (EDX) spectroscopy. Signals of phosphorous and sulfur dominate the EDX spectrum. Trace amounts of oxygen and carbon were also detected. The oxygen and carbon could be from the organic solvent. It is interesting that no fluorine was detected. This means bis(trifluoromethane)sulfonimide lithium salt (LiTFSI) does not contribute to the formation of the passivation layer as it does in Li-S batteries with $LiNO_3$ as the additive.[7] The atomic ratio of P to S is about 1:3.2. The passivation layer conducts lithium ions and functions as the solid electrolyte interphase (SEI) for the battery operations. **Figure 3**A shows the X-ray diffraction (XRD) pattern of the cycled lithium anode. Two strong peaks at 2 theta of 36.0° and 52.1° are the (011) and (002) peaks of crystalline lithium. A series of small peaks from 10 to 30° are identified as Li_2S, Li_3P, $Li_4P_2S_6$ and Li_3PS_4. The peak positions are assigned as the following: Li_2S, 27.3° (111); Li_3P, 22.7° (002), 26.4° (101); $Li_4P_2S_6$, 17.4° (100) and 27.3° (002); and Li_3PS_4, 12.2° (200), 14.6° (101), 20.3° (210), 21.4° (211), and 25.1° (220).[13] The Raman spectrum of the passivation layer in Figure 3B has remarkable peaks in the wavenumber ranging from 500 to 150 cm^{-1}. The predominate peak at 418 cm^{-1} is due to the symmetric stretching of the P-S bond in Li_3PS_4. Weak peaks of 305 and 229 cm^{-1} are from the stretching vibrations of the P-S bond in PS_4^{3-} ions with T_d symmetry.[14] Peaks at wavenumbers of 184 and 257 cm^{-1} are due to stretching vibrations of the P-S bond of $P_2S_6^{4-}$ ions.[15] The strong intensity of the peak at 418 cm^{-1} confirms that Li_3PS_4 is the major component of the passivation layer. Li_3PS_4 is a stable stoichiometric compound in the ternary phase diagram of the Li-P-S system.[16] This compound is a known lithium super-ionic conductor.[17] The passivation layer is highly conductive to lithium ions. A low voltage hysteresis of the charge/discharge loop in Figure 1B confirms that the resistance of ion transfer at the anode surface is low.

The electrochemical impedance spectra in Figure 3C show the resistivity at the end of the first discharge cycle. The cell without P_2S_5 has much higher resistivity than that of the one with P_2S_5. The difference of the cell resistivity rises from the difference of ionic conductivity of the SEI layers. Without P_2S_5, the SEI on the lithium anode is resulting from the chemical reaction of polysulfide with the lithium metal. The main component of the SEI is Li_2S, which is poor lithium ion conductor. With P_2S_5, the main component of the SEI is Li_3PS_4, which is a superionic conductor of lithium ions. The EIS data are consistent with the observation of low voltage hysteresis in Figure 1B.

Obviously, the passivation layer results from the chemical reactions between P_2S_5 and lithium metal. This passivation layer functions as a lithium ionic conductor that allows Li-ion transport to and from the Li anode surface and prevents the polysulfides from accessing and reacting with the Li anode. The protection of the lithium metal anode eliminates the polysulfide shuttle and results in the high coulombic efficiency during electrochemical cycling.

2.3. Complexes of Li_2S_x/P_2S_5 Facilitate the Redox Reactions

As observed in the control experiment, the cell capacity decreased rapidly in the first few cycles when a low surface area carbon was used as the host material for Li-S batteries. The capacity

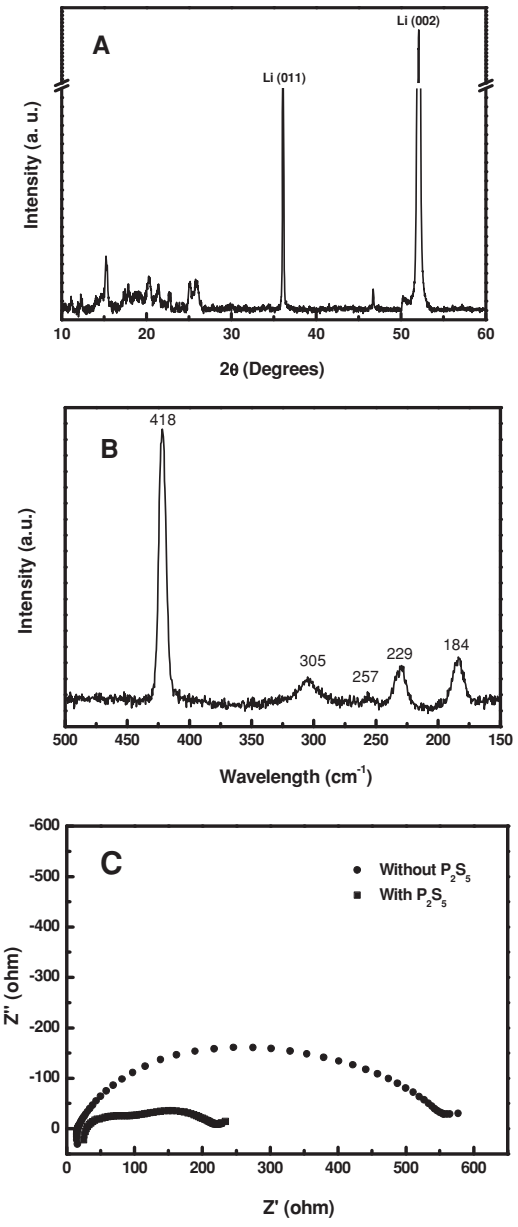

Figure 3. A) XRD pattern and B) Raman spectrum of the passivation layer on Li surface after the first cycle in 1 M LiTFSI solution in TEGDME with P_2S_5. C) The a.c. impedance measurements of Li-S batteries with and without P_2S_5 after the first discharge cycle.

decay is associated with the loss of sulfur species through the precipitation of lithium sulfide and disulfide.[9] Although the passivation of the lithium surface can improve the coulombic efficiency of the battery, the dramatic improvement of capacity retention in the experimental cell cannot be exclusively ascribed to the cessation of the polysulfide shuttle. There must be an additional mechanism functioning in the Li-S cell with P_2S_5. To reveal this mechanism, we started with a bench-top reaction of Li_2S with P_2S_5. The photo in **Figure 4** visually presents the solubility of a series of mixtures of Li_2S_x ($1 \le x \le 8$) with and without P_2S_5 in tetraethylene glycol dimethyl ether (TEGDME).

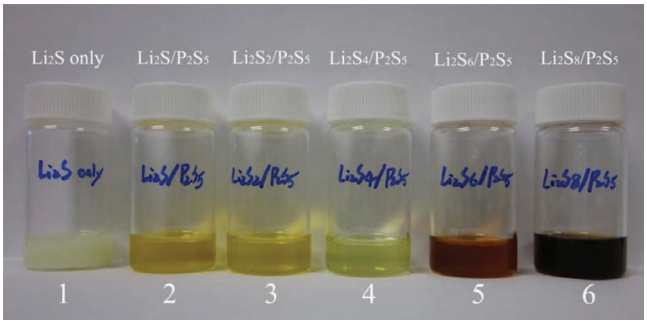

Figure 4. Photograph of 1) insoluble Li_2S and dissolved Li_2S_x/P_2S_5 (2. Li_2S/P_2S_5, 3. Li_2S_2/P_2S_5, 4. Li_2S_4/P_2S_5, 5. Li_2S_6/P_2S_5, and 6. Li_2S_8/P_2S_5) complexes in TEGDME. The weight ratio of solid to liquid in each vial is 1:10.

The weight ratios of solid to liquid in these vials are fixed at 1:10. The turbid mixture in the first vial showed that Li_2S is insoluble in TEGDME. With 1:1 molar ratio of Li_2S/P_2S_5 in the second vial, we found that the mixture was completely dissolved in TEGDME. The dissolution phenomenon was observed in all vials that contains Li_2S_x ($1 \le x \le 8$) and P_2S_5. The color of the complex depends on the length of the sulfur chain. The colors of long-chain polysulfides are darker than those of the short-chain polysulfides. Since P_2S_5 is a solid at room temperature, the enhanced solubility of Li_2S in TEGDME must be through a complex of Li_2S with P_2S_5. The retention of the cycling capacity of the experimental cell is attributed to the improved solubility of Li_2S and Li_2S_2 in TEGDME by forming complexes with P_2S_5.

The electrochemical properties of the Li_2S_x/P_2S_5 complexes were investigated by cyclic voltammography (CV). The blank CV of 0.1 M LiTFSI in TEGDME showed negligible current between 1.5 and 3.2 V at a scan rate of 100 mV s^{-1}. **Figure 5** shows the cyclic voltammograms of Li_2S/P_2S_5, Li_2S_6/P_2S_5, and Li_2S_8/P_2S_5 in TEGDME with 0.1 M LiTFSI as the supporting electrolyte. The scan rate was fixed at 100 mV s^{-1}. No redox peak was observed in the Li_2S/P_2S_5 complex between 1.7 and 3.2 V. This complex can be reduced at potentials below 1.7 V and be oxidized at potentials over 3.2 V. Obviously the formation of Li_2S/P_2S_5 does facilitate the electrochemical oxidation of Li_2S within the potential range of electrochemical cycling. So the improved cyclability of Li_2S might be associated with the high solubility of the Li_2S/P_2S_5 complex. Intuitively, chemical reactions between long-chain polysulfides and Li_2S can be accelerated in homogeneous solutions. The CV curves of Li_2S_6/P_2S_5 and Li_2S_8/P_2S_5 are quite similar. The onset of the reduction peak is at 2.4 V, which corresponds to the first plateau at the discharge curve. A reduction peak was observed at 2.0 V. This peak corresponds to the second plateau in the discharge curve. The peak representing the oxidation of long-chain polysulfides (Li_2S_x, $x \ge 4$) starts at 2.5 V, which agrees with the second plateau of the charging cycle. The CV results are consistent with the voltage profiles of the electrochemical cycling.

3. Conclusions

In summary, we found that P_2S_5 forms complexes with Li_2S_x ($1 \le x \le 8$). This reaction converts the less soluble species of

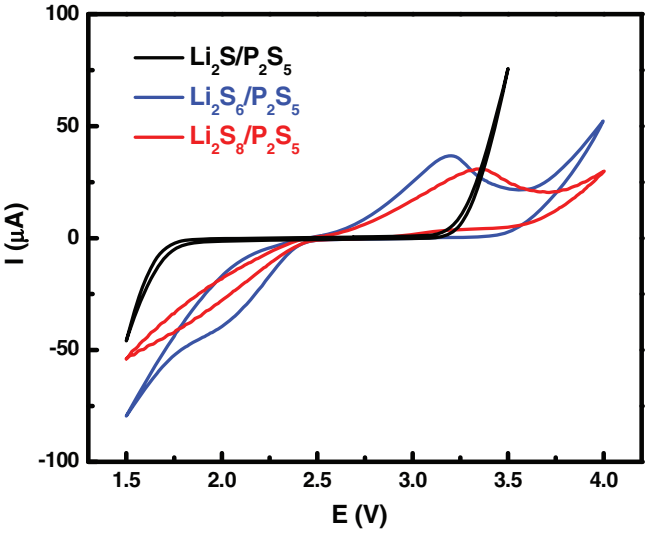

Figure 5. Cyclic voltammograms of 10 wt% Li_2S_x/P_2S_5 ($x = 1$, 6, and 8) in TEGDME with 0.1 M LiTFSI as the supporting electrolyte. The scan was conducted at 100 mV s^{-1}.

Li_2S and Li_2S_2 into highly soluble complexes with P_2S_5. Cyclic voltammogram showed that P_2S_5 is electrochemically stable between 1.7 and 3.2 V versus lithium. The capacity retention of cycling Li-S battery was greatly improved when P_2S_5 was used as an electrolyte additive. The enhanced solubility of Li_2S in organic electrolyte is accountable for improvements of battery cycling.

P_2S_5 has been identified as the critical chemical of forming a passivation layer on the surface of lithium metal anode. The major component of the passivation layer is Li_3PS_4. The passivation layer functions as the solid electrolyte interphase with a dense structure that is able to conduct lithium ions while preventing access of the polysulfide to the surface of the metallic lithium. The protection of the lithium surface blocks the polysulfide shuttle and thus results in a high coulombic efficiency for battery cycling. The long-term stability of the passivation layer is still under investigation; it would be extremely valuable to the research field if the passivation layer can mitigate the long-standing problem of dendritic growth of lithium metal anode.

4. Experimental Section

Chemicals and Reagents: Lithium sulfide (Li_2S), phosphorus pentasulfide (P_2S_5), sulfur (S), bis(trifluoromethane)sulfonimide lithium salt (LiTFSI, 99.95% trace metals basis), and tetraethylene glycol dimethyl ether (TEGDME) were purchased from Sigma-Aldrich and were used without further purification.

Cyclic Voltammography: A solution was prepared as 10 wt% Li_2S_x/P_2S_5 and 0.1 M LiTFSI in TEGDME. A mild ultra-sonication was employed to accelerate the dissolution of solids. All solids can be dissolved within a few minutes. Cyclic voltammography was performed on a potentiostat (EG&G) at a scan rate of 100 mV s^{-1} at room temperature using the above solution in a three-electrode cell, which consists of a working electrode (glassy carbon), a counter electrode (Pt wire), and a reference electrode (metallic Li). A blank CV test of 0.1 M LiTFSI in TEGDME was conducted at identical conditions.

Electrochemical Evaluation: Swagelok cells were used to evaluate the cycling performance. Low surface area carbon black (surface area ≈50 m^2 g^{-1}) coated aluminum foil (10 mm in diameter) was used as the current collector of the sulfur cathode. Sulfur was loaded on to the cathode by using a 10 wt% sulfur solution in carbon disulfide. A lithium foil (10 mm in diameter) was used as the anode. The anode and cathode were separated by a Celgard 3225 separator (10.3 mm in diameter). The organic electrolyte was the solution of 1 m LiTFSI in TEGDME. P_2S_5 was added to the electrolyte in format of Li_2S/P_2S_5 complex with a molar ratio of 1:1. The electrolyte of the experimental cell contained 5 wt% of Li_2S/P_2S_5 complex. The amount of electrolyte was defined by the voids of the separator and the cathode. A total volume of 2 μL electrolyte was used in each cell. The cathode, separator, and anode were pressed by a spring to ensure tight contact, without an excess of electrolyte left in the assembled cell. The control experiment was conducted under identical conditions except for the electrolyte, which did not contain Li_2S/P_2S_5 complex. Charge and discharge were carried out using a Maccor 4000 series battery tester at a current density of 0.125 mA cm^{-2} (0.1 C) between the cut-off potentials of 1.7–3.2 V vs. Li/Li^+. The cut-off current for the charge cycle was set to 0.0125 mA cm^{-2}. The calculation of specific discharge capacities is based on the mass of elemental S.

Electrochemical Impedance Spectroscopic Study: The a.c. impedance measurements were conducted in the frequency range of 10 MHz to 1 Hz with the amplitude of 10 mV by using a frequency response analyzer (Solartron 1260). Two fresh cells, one with and one without P_2S_5 were discharged to 1.7 V at a current density of 0.125 mA cm^{-2}. The EIS data was taken immediately after the cell potential reached 1.7 V.

Structure Characterization: The structures of Li surface before and after cycling were examined using a field emission STEM (Hitachi HF-3300) at 15 kV. The thickness of the passivation layer on the Li surface was determined using an ImageJ software package. X-ray diffraction (XRD) analysis was performed at a PANalytical X'pert PRO2-circle X-ray diffractometer with a CuKα radiation ($\lambda \approx 1.5418$ Å). The operating voltage and current were 45 kV and 40 mA, respectively. Raman spectroscopy was recorded from 600 to 100 cm^{-1} on a Renishaw Confocal MicroRaman spectrometer at room temperature.

Acknowledgements

This research was sponsored by U.S. Department of Energy (DOE)/Energy Efficiency and Renewable Energy (EERE) through Vehicle Technology Program. The Raman, EIS, and XRD characterization of the solid electrolyte interphase on the lithium metal surface was supported by the Division of Materials Science and Engineering, Office of Basic Energy Sciences U.S. Department of Energy (DOE). The synthesis and characterization was conducted at the Center for Nanophase Materials Sciences, which is sponsored at Oak Ridge National Laboratory by the Scientific User Facilities Division, Office of Basic Energy Sciences, U.S. DOE.

Received: March 13, 2012
Revised: May 9, 2012
Published online: June 14, 2012

[1] a) J. B. Goodenough, Y. Kim, *Chem. Mater.* **2010**, *22*, 587; b) Z. Liu, W. Fu, C. Liang in *Lithium–Sulfur Batteries*, Vol. *2* Wiley-VCH Verlag & Co. KGaA, Weinheim, Germany **2011**, p. 811; c) B. Scrosati, J. Garche, *J. Power Sources* **2010**, *195*, 2419.
[2] a) A. S. Arico, P. Bruce, B. Scrosati, J. M. Tarascon, W. Van Schalkwijk, *Nat. Mater.* **2005**, *4*, 366; b) B. L. Ellis, K. T. Lee, L. F. Nazar, *Chem. Mater.* **2010**, *22*, 691; c) L. W. Ji, Z. Lin, M. Alcoutlabi, X. W. Zhang, *Energ. Environ. Sci.* **2011**, *4*, 2682; d) M. R. Palacin, *Chem. Soc. Rev.* **2009**, *38*, 2565.
[3] Y. V. Mikhaylik, J. R. Akridge, *J. Electrochem. Soc.* **2004**, *151*, A1969.

[4] a) X. L. Ji, S. Evers, R. Black, L. F. Nazar, *Nat. Commun.* **2011**, *2*,325; b) X. L. Ji, K. T. Lee, L. F. Nazar, *Nat. Mater.* **2009**, *8*, 500; c) R. Demir-Cakan, M. Morcrette, F. Nouar, C. Davoisne, T. Devic, D. Gonbeau, R. Dominko, C. Serre, G. Ferey, J. M. Tarascon, *J. Am. Chem. Soc.* **2011**, *133*, 16154; d) N. Jayaprakash, J. Shen, S. S. Moganty, A. Corona, L. A. Archer, *Angew. Chem. Int. Ed.* **2011**, *50*, 5904; e) C. Lai, X. P. Gao, B. Zhang, T. Y. Yan, Z. Zhou, *J. Phys. Chem. C* **2009**, *113*, 4712; f) C. D. Liang, N. J. Dudney, J. Y. Howe, *Chem. Mater.* **2009**, *21*, 4724; g) J. Shim, K. A. Striebel, E. J. Cairns, *J. Electrochem. Soc.* **2002**, *149*, A1321; h) M. S. Song, S. C. Han, H. S. Kim, J. H. Kim, K. T. Kim, Y. M. Kang, H. J. Ahn, S. X. Dou, J. Y. Lee, *J. Electrochem. Soc.* **2004**, *151*, A791; i) B. Zhang, X. Qin, G. R. Li, X. P. Gao, *Energy Environ. Sci.* **2010**, *3*, 1531; j) J. C. Guo, Y. H. Xu, C. S. Wang, *Nano Lett.* **2011**, *11*, 4288; k) Y. L. Cao, X. L. Li, I. A. Aksay, J. Lemmon, Z. M. Nie, Z. G. Yang, J. Liu, *Phys. Chem. Chem. Phys.* **2011**, *13*, 7660.

[5] L. W. Ji, M. M. Rao, H. M. Zheng, L. Zhang, Y. C. Li, W. H. Duan, J. H. Guo, E. J. Cairns, Y. G. Zhang, *J. Am. Chem. Soc.* **2011**, *133*, 18522.

[6] Y. V. Mikhaylik, U.S. Patent 7354280, **2008**.

[7] D. Aurbach, E. Pollak, R. Elazari, G. Salitra, C. S. Kelley, J. Affinito, *J. Electrochem. Soc.* **2009**, *156*, A694.

[8] a) X. Liang, Z. Y. Wen, Y. Liu, M. F. Wu, J. Jin, H. Zhang, X. W. Wu, *J. Power Sources* **2011**, *196*, 9839; b) G. Y. Zheng, Y. Yang, J. J. Cha, S. S. Hong, Y. Cui, *Nano Lett.* **2011**, *11*, 4462; c) S. S. Zhang, J. A. Read, *J. Power Sources* **2012**, *200*, 77.

[9] S.-E. Cheon, S.-S. Choi, J.-S. Han, Y.-S. Choi, B.-H. Jung, H. S. Lim, *J. Electrochem. Soc.* **2004**, *151*, A2067.

[10] a) J. Hassoun, B. Scrosati, *Angew. Chem. Int. Ed.* **2010**, *49*, 2371; b) Y. Yang, M. T. McDowell, A. Jackson, J. J. Cha, S. S. Hong, Y. Cui, *Nano Lett.* **2010**, *10*, 1486.

[11] a) A. Hayashi, R. Ohtsubo, T. Ohtomo, F. Mizuno, M. Tatsumisago, *J. Power Sources* **2008**, *183*, 422; b) Y. N. Zhou, C. L. Wu, H. Zhang, X. J. Wu, Z. W. Fu, *Electrochim. Acta* **2007**, *52*, 3130.

[12] a) C. D. Liang, N. Dudney, J. Y. Howe, U.S. Patent 61/239,132, **2010** ; b) R. F. Service, *Science* **2011**, *332*, 1494.

[13] T. Sotomura, H. Uemachi, K. Takeyama, K. Naoi, N. Oyama, *Electrochim. Acta* **1992**, *37*, 1851.

[14] a) F. Mizuno, A. Hayashi, K. Tadanaga, M. Tatsumisago, *Adv. Mater.* **2005**, *17*, 918; b) A. Muller, N. Mohan, P. Cristoph, I. Tossidis, M. Drager, *Spectrochim. Acta A* **1973**, *A29*, 1345.

[15] a) W. Carrillocabrera, J. Sassmannshausen, H. G. Vonschnering, F. Menzel, W. Brockner, *Z. Anorg. Allg. Chem.* **1994**, *620*, 489; b) A. V. Gomonnai, Y. M. Azhniuk, Y. M. Vysochanskii, A. A. Kikineshi, M. Kis-Varga, L. Daroczy, I. P. Prits, I. M. Voynarovych, *J. Phys.: Condens. Matter* **2003**, *15*, 6381.

[16] M. Murayama, N. Sonoyama, A. Yamada, R. Kanno, *Solid State Ionics* **2004**, *170*, 173.

[17] a) A. Hayashi, *J. Ceram. Soc. Jpn.* **2007**, *115*, 110; b) A. Hayashi, *Glass Technol.: Part A* **2008**, *49*, 213; c) K. Homma, M. Yonemura, T. Kobayashi, M. Nagao, M. Hirayama, R. Kanno, *Solid State Ionics* **2011**, *182*, 53.